CrystEngComm

Synthesis of Luminescent Lanthanide Complexes within Crosslinked Protein Crystal Matrices

Journal:	*CrystEngComm*
Manuscript ID	CE-ART-02-2018-000318.R1
Article Type:	Paper
Date Submitted by the Author:	20-Mar-2018

Complete List of Authors:	Zhang, Yu; Qingdao University, Matertials Science and Engineering Zhang, Xiaoting; Qingdao University, Matertials Science and Engineering Tang, Jianguo; Qingdao University, Matertials Science and Engineering Snow, Christopher; Colorado State University, Chemical and Biological Engineering Sun, Guotao; Qingdao University, Matertials Science and Engineering Kowalski, Ann; Colorado State University, Chemical and Biological Engineering Hartje, Luke; Colorado State University College of Natural Sciences, Biochemistry Zhao, Ning; Colorado State University College of Natural Sciences, Biochemistry Wang, Yao; Qingdao University, Materials Science and Engineering Belfiore, Laurence; Colorado State University, Chemical & Biological Engineering

Journal Name

ARTICLE

Synthesis of Luminescent Lanthanide Complexes within Crosslinked Protein Crystal Matrices

Received 00th January 20xx,
Accepted 00th January 20xx

DOI: 10.1039/x0xx00000x

www.rsc.org/

Yu Zhang[a], Xiaoting Zhang[a], Jianguo Tang*[a], Christopher D. Snow*[bc], Guotao Sun[a], Ann E. Kowalski[b], Luke F. Hartje[c], Ning Zhao[c], Yao Wang[a], Laurence A. Belfiore[ab]

Crosslinked protein crystals offer unique properties as a host matrix for hybrid materials, due to their precise periodic array of solvent channels suitable for the capture of functional guest molecules. To prepare luminescent protein crystals containing guest Eu(TTA)$_3$phen (TTA=4,4,4-trifluoro-1-(2-thienyl)-1,3-butanedionato, phen=1,10-phenanthroline), we developed a solvent substitution scheme in which the crystals were first loaded with the hydrophobic ligands and subsequently loaded with Eu(III) in anhydrous ethanol. Notably, we also observed crystal denaturation and renaturation, concomitant with a dramatic volume expansion, in response to high DMSO concentrations. Given the possible future utility of this reversible expansion for hybrid materials preparation, we characterized the volumetric changes quantitatively.

Introduction

For long-term photonics applications, precise control over the interactions between light and materials will be required. Ultimate control will include the ability to place functional groups that adsorb or emit light at varying positions in 3-dimensions with precise control over position and orientation. The ideal scaffold to enable programmed placement of functional groups in 3-D will also facilitate validation via high-resolution structure determination. Crystalline scaffolds suitable for single-crystal X-ray diffraction may therefore be ideal. Within this category, metal-organic frameworks, covalent-organic frameworks, DNA crystals, and protein crystals may serve as crystalline scaffolds. DNA and protein crystals are interesting candidates because of their porosity, their high spatial density of functional groups, and because it should often be possible to make site-specific modifications to the materials via molecular biology or chemical biology methods.[1-6]

Bimolecular crystals do have limitations to their broader use as materials. First, it is difficult to master the highly sensitive nucleation and growth conditions associated with crystal growth. Second, conventional crystals have limited size range (microns to millimeters). Third, protein production and purification at a typical laboratory scale can be expensive and time consuming. These challenges can be addressed by using an economical protein like hen egg white lysozyme (HEWL) with well-known crystal growth conditions. The last barrier to the use of protein crystals as materials is the limited mechanical and solvent stability of the as-grown crystals. Fortunately, protein crystals can easily be stabilized via chemical crosslinking.[7, 8] By adding covalent bonds between neighboring proteins, agents like glutaraldehyde can convert fragile non-covalent crystals into materials that are robust with respect to temperature, acid, base, mechanical trauma, or solvent changes as demonstrated herein.

Luminescent lanthanide complexes (LC) are one interesting class of guest molecules with excellent photonic properties including long luminescence lifetime, narrow emission peak, large Stokes shift, and a peak emission wavelength that changes minimally with ligands.[9-16] LC can be synthesized easily and different lanthanide atoms emit different wavelengths of visible light via photoluminescence. The favourable photo-physical properties of LC are due to forbidden f-f electron transitions. However, the forbidden f-f transitions also cause unfavourable low absorption efficiency. To overcome this barrier, we rely on an optimized LC, Eu(TTA)$_3$phen, in which the ligand molecules serve as molecular "antenna". Specifically, TTA and phen not only (1) possess triplet states with energy equal to or higher than the resonance level of the Europium trivalent ion, but also (2) overlap their emission spectrum with absorption spectrum of the lanthanide ion. Eu(TTA)$_3$phen yields intense and efficient emission by transferring the energy of the ligands to the central emitting ion, a process called intersystem crossing.

Given the advantageous properties of LC, numerous researchers have developed methods for embedding LC within

[a] Institute of Hybrid Materials, National Center of International Research for Hybrid Materials Technology, National Base of International Science & Technology Cooperation, College of Materials Science and Engineering, Qingdao University, Qingdao, 266071, P. R. China. Email: tang@qdu.edu.cn
[b] Department of Chemical and Biological Engineering, Colorado State University, Fort Collins, Colorado 80523 USA. Email: Christopher.Snow@colostate.edu
[c] Department of Biochemistry and Molecular Biology, Colorado State University, Fort Collins, Colorado 80523 USA. Email: Christopher.Snow@colostate.edu

Electronic Supplementary Information (ESI) available: [details of any supplementary information available should be included here]. See DOI: 10.1039/x0xx00000x

a variety of host materials including agricultural light conversion film[17], novel colour display devices[11], and fluorescent anti-counterfeiting fiber[18]. Here we take the initial steps to evaluate the possibility of using protein crystals as a host material for guest LC. In principle, an ideal host material might maximize the economy and efficiency of light emitting functional groups by controlling the spacing and orientation of those groups. Depending on the fluorophore, such control might help prevent aggregation and unfavourable phenomena such as aggregation-induced quenching.

Given the potential benefits of crosslinked protein crystals as stable yet precise scaffold materials discussed above, several research groups have explored the use of protein crystals as biotemplates[19, 20], reaction vessels[21, 22] or host materials for guest molecules. The most similar existing work to the present study comes from Mann[23-25] and coworkers and Cvetkovic et al.[26]. Specifically, cross-linked lysozyme crystals (CLLCs) were used as a highly porous matrix for the subsequent capture of small molecules such as bromophenol blue[23] and xanthene dyes [26]. Additionally, Mann and coworkers used CLLCs as the host materials for the synthesis of carbon dots[24] and nanoplasmonic arrays thereof[25] within the solvent channels. To our knowledge, no group has reported the loading of pre-formed LC into CLLCs nor the synthesis of LC inside the internal solvent spaces of CLLCs.

Disparate solvent requirements are a common challenge for hybrid materials in general and are certainly a challenge for the simultaneous use of LC and protein crystals. Whereas proteins are typically soluble and stable in aqueous solvents, many LC, including the highly luminescent LC used here, $Eu(TTA)_3phen$, aggregate rapidly in aqueous solvents. To maximize the versatility of protein crystals as a scaffold material it is necessary to develop processing methods that can work with functional guest molecules that are only soluble in organic solvents.

In this study, we developed a multi-stage protocol for the assembly of luminescent LC inside of host HEWL crystals. We have successfully synthesized our target materials using two solvents, ethanol and dimethyl sulfoxide (DMSO). Briefly, HEWL crystals were thoroughly cross-linked with glutaraldehyde, washed, then incubated in either ethanol or DMSO with TTA and phen (at pH ~7.4). After crystals had adsorbed the hydrophobic antenna ligands, they were physically transferred to $EuCl_3$ ethanol solution (Methods). This setup has the potential, depending on adsorption and diffusion kinetics, to result in a complex counter-diffusion process. In practice, we could use fluorescence microscopy to observe the dramatic increase in luminescence accompanying the formation of $Eu(TTA)_3phen$ inside the host crystals.

An additional fascinating aspect of the DMSO solvent substitution process was the sizable physical expansion of CLLCs when they were soaked in DMSO or aqueous solutions containing high DMSO concentration (≥ 60 vol% DMSO). David Haas[27] and Ada Yonath[28, 29] previously studied crystal expansion via denaturation and renaturation for cross-linked HEWL crystals in several denaturants, such as bromoethanol, guanidinium chloride, urea, lithium chloride and sodium dodecyl sulfate. However, to our knowledge, the present work provides the first example of partially reversible, DMSO-induced crystal expansion. Notably, we characterized the cross-linked HEWL crystals by SEM, allowing us to visualize the micro-fractures that resulted from the expansion and contraction process.

Method and materials

Reagents and solutions

The following chemicals were obtained and used without further purification. Lyophilized hen egg white lysozyme (HEWL) and Lysozyme Crystallization Solution (HR2-805, 30% w/v MPEG5000, 1.0 M sodium chloride, 0.05 M sodium acetate tri-hydrate pH 4.6) were purchased from Hampton Research, Inc. 2-thenoylthrifluoroacetone (TTA, ≥98%) was purchased from Shanghai Macklin Biochemical Company. 1,10-phenanthroline ($C_{12}H_8N_2$, Analytical Reagent(AR)), anhydrous ethanol (CH_3CH_2OH, AR), ammonia solution (NH_3, AR), and europium(III) oxide (Eu_2O_3, ≥ 99.99%) were purchased from Sinopharm Chemical Reagent company. Hydrochloric acid (HCl, AR) was purchased from Yantai Shuangshuang Chemical Company. Sodium acetate tri-hydrate was purchased from BASF SE (Tianjin, P.R. China). Dimethyl sulfoxide (DMSO, AR) was purchased from Tianjin Fuyu Fine Chemical Company. Glutaraldehyde (≥50%) was purchased from Tianjin Bodi Chemical Company.

HEWL Crystal Growth

Crystals were grown via vapor diffusion using 24-well Cryschem sitting drop plates purchased from Hampton Research. HEWL was resuspended in a buffer containing 0.02 M sodium acetate tri-hydrate aqueous solution with the pH value adjusted to 4.6 using glacial acetic acid. We obtained the best crystal growth using HEWL stock solutions at 30 mg/mL and 50 mg/mL. After reservoirs on the plate were filled with 400 microliters of Lysozyme Crystallization Solution, 5 microliters of protein buffer and 5 microliters of reservoir solution were pipetted into each concave well. Finally, each well was rapidly sealed with Crystal Clear Sealing Tape and incubated at 20℃ for 24 hours.

Washing Process

The washing solution was made by mixing 80 vol% reservoir solution with 20 vol% ultrapure water. To wash the crystals, 10 µL of washing solution was added to each crystal growth drop for 10 minutes. Then crystals were quickly transferred into another well containing exclusively 20 µL washing solution. After a brief incubation (less than one minute) the crystals were again transferred to a new well for crosslinking.

Cross-Linking

Our cross-linking buffer was the reservoir solution mixture supplemented with 4 vol% glutaraldehyde. No more than twenty washed lysozyme crystals with length about 100 µm were manually transferred into 20 µL of cross-linking reagent

in a new well and sealed at room temperature for 24 hours to promote uniform crosslinking. Cross-linked crystals were subsequently transferred into a drop containing reservoir solution for storage.

In addition to the direct addition of glutaraldehyde, we also attempted glutaraldehyde vapor diffusion as described by Lusty et al.[7]. Specifically, 2 µL of glutaraldehyde solution was pipetted on the sticky side of sealing tape and incubated for 24 hours above crystals soaking in 20 µL reservoir solution at room temperature. In our hands, crystals produced by the vapor diffusion crosslinking method were less uniformly cross-linked. Crystals with non-uniform crosslinking experienced non-uniform expansion when soaked in DMSO, which increased the difficulty of quantifying crystal dimensions.

Denaturation and Renaturation

Denaturation: Individual CLLCs were physically transferred using a Cryo-Loop (Hampton Research) from the mother liquor crystallization solution and incubated and sealed in 30 µL of 20 vol% DMSO aqueous solution for 5 hours in a sitting drop plate with 400 µL 20 vol% DMSO aqueous solution in the reservoir. The same CLLC was serially transferred and incubated in aqueous DMSO solutions with increasing DMSO concentration (40%, 60 vol%) for 5 hours at each concentration. For the final two concentrations (80%, 100 vol%, DMSO) we used a 2-hour incubation time to ensure that crystal size had equilibrated. We selected these incubation times after observing crystal size versus time (Fig.S1).

Renaturation: We directly used the same batch of CLLC that had been through the gradual denaturation process and incubated them in 30 µL drops with stepwise reduced DMSO concentration (80%, 60%, 40%, 20vol%). Each incubation step was over 12 hours in a 30 µL drop (with a corresponding 400 µL DMSO aqueous solution in the reservoir). For the final incubation, we used the crystallization solution rather than distilled water.

Eu(TTA)$_3$phen Synthesis in Solution

Europium chloride hexahydrate crystals were prepared by dissolving europium oxide in excess hydrochloric acid and moderately stirring at 60℃ for 10 hours to crystallize Europium (III) chloride hexahydrate. After drying in vacuum at 40℃ for one day, Europium (III) chloride hexahydrate was dissolved in anhydrous ethanol. The ligand solution was made by dissolving TTA and phen in either anhydrous ethanol or DMSO at a molar ratio of 3:1, and adjusting pH to 7.4 with 2M ammonia. For LC synthesis in solution, a stoichiometric quantity of $EuCl_3$ was added to the ligand solution dropwise with simultaneous stirring at ambient temperature for 1 hour.

Attempted Loading of Pre-Assembled Eu(TTA)$_3$phen Into Cross-linked HEWL Crystals:

Based on our empirical results, Eu(TTA)$_3$phen prepared in solution as described above had a strong tendency to aggregate in water, and a moderate tendency to aggregate in other solvents such as ethanol, DMSO or acetone. When we incubated both pre-assembled Eu(TTA)$_3$phen and CLLCs in ethanol, only LC aggregation on the crystal surfaces was observed rather than uptake into the body of the crystals (Fig. S2). Results were similar when we replaced the ethanol solvent with DMSO.

Assembly of Eu(TTA)3phen inside HEWL Crystals:

Via anhydrous ethanol and DMSO:

Since pre-assembled Eu(TTA)$_3$phen aggregated on the surface of the HEWL crystals rather than diffusing into the body, we decided to pursue a novel option: assembly inside the crystals. A phen and TTA ligand solution was prepared by mixing a DMSO solution with 30 mM TTA and 10 mM phen that was adjusted to pH 7.4 with 2M ammonia. Fewer than five CLLCs at a time were sealed in 30 µL ligand solution drops in a well on a sitting drop plate for 2 hours. These crystals were next transferred to a 30 µL, 10 mM $EuCl_3$ ethanol solution for no more than 5 minutes. These Eu(TTA)$_3$phen-doped CLLCs were quickly washed by anhydrous ethanol and dried in vacuum at room temperature.

Via anhydrous ethanol:

A ligand solution was prepared by mixing equal volumes of 30 mM TTA and 10 mM phen anhydrous ethanol solution, with pH adjusted to 7.4 by 2M ammonia. Fewer than five CLLCs at a time were sealed in 30 µL ligand solution drops in a sitting drop plate well for 2-7 days. Depending on the ligand loading conditions (the time length of incubation of ligand anhydrous ethanol solution), we tested two protocols to introduce Eu^{3+}. After more than 5-day-incubation, crystals were subsequently transferred to a 30 µL drop containing 10 mM $EuCl_3$ ethanol solution for at least 30 minutes. Another batch of crystals, incubated for less than 3 days were first transferred to a 0.1 M $EuCl_3$ ethanol solution and incubated for at least 30 minutes, then incubated in 10 mM $EuCl_3$ ethanol solution for at least 30 minutes. The resulting Eu(TTA)$_3$phen-doped CLLCs were quickly washed by anhydrous ethanol and dried in vacuum at room temperature.

Quantifying HEWL Crystal Dimensions:

To image the crystals we used a stereo-zoom microscope (Chongqing Aote Optical Instrument Co., Ltd.) with a 5-megapixel camera (AOR). We measured crystal dimensions using software (AJ-VERT) supplied with the camera. To approximate the macro-volume of each tetragonal crystal we measured the crystal width and height with details given in Fig. S3. Briefly, we applied the following formula: $V \approx A_{top} \cdot \frac{H_1+H_2}{2}$. Here, A_{top} represents the measured cross-section area of each tetragonal HEWL crystal from the top view down the 4-fold symmetry axis. From this view, we can see only the 101, $0\bar{1}1$,$\bar{1}$01 and 011 facets (Fig. S4a). To measure the height of the crystal, perpendicular to the A_{top} plane, we turn the crystal on its side. H_2 represents the height of the edges that join the $1\bar{1}0$, 110, $\bar{1}10$, and $1\bar{1}\bar{0}$ facets while H_1 is the maximum height of

the crystal along the central 4-fold axis, as assessed from all four side views (Fig. S4b-e).

Results and discussion

To visualize the major solvent channels in tetragonal ($P4_32_12$) lysozyme crystals we started with a high-resolution (1.33Å) HEWL structure (pdb code: 193L).[30] We then used the map_channels_v0.5 software[31] to generate a "cast" of the solvent channels by placing dummy atoms on 1 Å grid. Notably, this software estimates a maximum stationary guest sphere radius of 7.02 Å and a maximum radius of 5.88 Å for guest molecules to diffuse along the z-axis. For visual analysis, we pruned this cast by excluding all grid points that were less than 4 Å from a protein atom and by manually excluding all grid points that were not contiguous with the major pores. We completed the visualization in PyMOL (The PyMOL Molecular Graphics System, Version v1.7.4.4 Schrödinger, LLC.) using a smooth Gaussian surface representation for the solvent channels (b=50, q=1, 1 Å grid, 6 Å buffer, 0.1 iso-surface level). Coordinates for two $Eu(TTA)_3phen$ enantiomers were obtained from the crystal structure reported by Hu et al.[32] The $Eu(TTA)_3phen$ crystal structure enantiomers are shown as spheres atop Fig. 1a. The pair of $Eu(TTA)_3phen$ atoms that are farthest apart are 12.8 Å. To demonstrate that $Eu(TTA)_3phen$ can (barely) fit within the solvent cavities we manually generated four poses for one enantiomer that fit within the approximate envelope of the major solvent channel (Fig. 1b) and further tuned these rigid body LC poses to avoid steric clashes with the constellation of neighboring protein atoms (green) that delimit the solvent channel (Fig. 1c). Only certain LC orientations fit for particular solvent channel locations. To the extent to which diffusion of intact $Eu(TTA)_3phen$ is feasible, diffusion may be contingent on conformational flexibility of the LC or the neighboring protein. Given the close correspondence between the size of $Eu(TTA)_3phen$ and the CLLC pores, any diffusion will not be of the classical Knudsen type. Instead, we expect diffusion to induce specific orientations of the guest molecules in which the longer molecular axis is aligned to the pores.

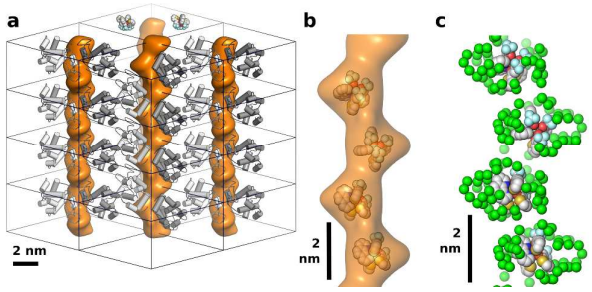

Figure 1. (a) A 2×2×4 collection of unit cells, with a narrow depth of field for clarity (most foreground and background HEWL copies were hidden). (b) Example poses for one LC enantiomer that fit within the approximate envelope of the major solvent channel. (c) Example poses for one LC enantiomer that fit within the constellation of neighboring protein atoms (green).

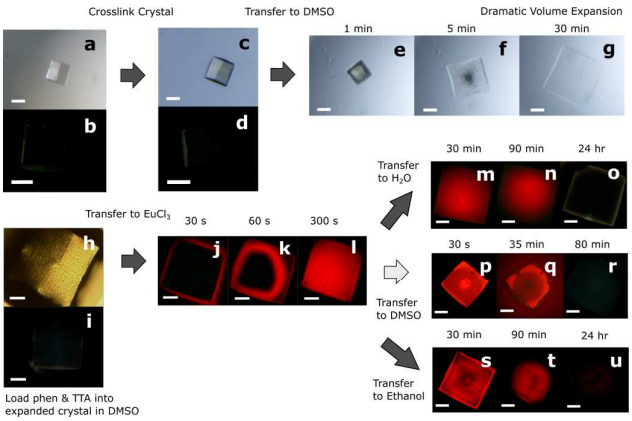

Figure 2. optical microscopy (a, c, e-g, h) and fluorescence microscopy (excitation wavelength is at the range of 330-400 nm) (b, d, i-u) images of CLLCs at different stages of loading TTA and phen in DMSO (h, i) and loading Eu(III) in ethanol (j-l), followed by $Eu(TTA)_3phen$ release in H_2O (m-o), DMSO (p-r), and ethanol (s-u). The scale bars, 100μm.

Native HEWL crystals were almost transparent and easily fragmented during manual manipulation (Fig. 2a), with minimal auto-fluorescence under UV illumination (Fig. 2b). To withstand the process of LC doping, increased robustness for the crystals is essential. We used glutaraldehyde, the most commonly reported crosslinking agent for protein crystals[33], to stabilize the HEWL crystals via conversion to crosslinked lysozyme crystals (CLLCs). CLLCs were faint yellow in white light (Fig. 2c) and often would faintly emit broad spectrum blue and green light (Fig. 3f) [34] under the same UV illumination condition as Fig. 2b (Fig. 2d).

Once CLLCs were transferred into 100% DMSO, a dramatic volume expansion occurred (in minutes, Fig. 2e-g). Expansion began with the crystal exterior, and proceeded as the DMSO penetrated the crystal interior. In the first few minutes, CLLCs developed a fine network of surface cracks (Fig. 2e). Next, the CLLCs began to swell from the edges, with the crack network converting to small bubbles (Fig. 2f). Eventually the bubbles vanished with final CLLC volumes about 2-3 times that of the original (Fig. 2g). Not much is known about the conformation of the denatured yet cross-linked monomers within the expanded crystal. Due to the macroscopic volume expansion, we assume that the monomers must occupy a greater volume commensurate with conversion of the compact folded HEWL domains to larger unfolded structures. After swelling, the stress within the crystal appears to be equilibrated such that the expanded crystal habit is similar to the original crystalline matrix. As discussed below, this process was approximately reversible.

We noted and took advantage of the reversible CLLC expansion phenomenon to facilitate *in* crystallo $Eu(TTA)_3phen$ synthesis. First, we dissolved stoichiometric ligand quantities (10mM phen and 30mM TTA) in DMSO, then added CLLCs (Fig. 2h, 2i). Once CLLCs were equilibrated in the expanded state, we extracted the swollen CLLCs using a loop and transferred them into 10mM $EuCl_3$ ethanol solution. As soon as a swollen, ligand-loaded CLLC was placed into the $EuCl_3$ in ethanol

solution, intense fluorescence from newly formed Eu(TTA)$_3$phen could immediately be observed. As expected, the spatial pattern for LC formation was complex, reflecting guest adsorption, the potential counter diffusion of the ligands and Eu(III), the expected reduced diffusion rate for the larger LC, and the concurrent volume decrease accompanying the partial renaturation of the crystal. Typically, we assumed the visible diffusion front corresponded to Eu^{3+} gradually infiltrating the crystal from the edges. Eventually the whole crystal emitted bright red light (Fig. 2j-l). The final uniformity was fairly high, though crystal vertices tended to be less bright, presumably due to the increase rate of LC escape to the surrounding solvent from these crystal extremities.

Depending on the long-term application, it is important to also characterize the rate at which LC can escape the CLLC. In one instance, LC-loaded crystals were left dried for multiple weeks. In this case, no significant loss of luminescence was observed via confocal microscopy during 3 hr of incubation in 100% ethanol. To test the stability of guest adsorption in freshly prepared crystals, we selected distilled water, DMSO and anhydrous ethanol as solvents (Fig. 2m-u). Fluorescence microscope images revealed DMSO possessed a much higher solvent-dependent release rate than distilled water or anhydrous ethanol. We speculate that the greater solubility of Eu(TTA)$_3$phen in DMSO compared to distilled water or anhydrous ethanol increased the LC release rate. Physical expansion of the crystals in DMSO could also increase guest molecule diffusion dramatically[35, 36]. Intrigued by the crystal denaturation and renaturation process, we proceeded to verify that the same LC loading and release process could be repeated with the same crystal. In our tests, CLLCs could usually survive at least 2 cycles of LC loading routine and release before rupture.

Notably, it was possible to obtain LC infiltrated crystals without the DMSO solvent exchange procedure. When we soaked CLLCs in a solution of 10 mM phen and 30 mM TTA in anhydrous ethanol instead of DMSO at pH about 7.4, lengthy incubations were needed to make a LC infiltrated crystal. Ligands (0.01M) in anhydrous ethanol gradually penetrated into the crystal on a multi-day timescale as assessed via a distinctive colour change (Fig. S5). Notably, the final fluorescence intensity of these crystals after Eu(III) loading was much higher than the fluorescence of comparable crystals prepared using the DMSO expansion stage. In the ethanol process, no obvious volume changes for the CLLCs were observed via the optical stereo microscope of CLLCs. The difference in ligand loading in ethanol was also apparent via light adsorption. Highly loaded crystals had a distinctly darker yellow colour (Fig. S5), suggesting a high concentration of antenna ligands, adsorbed throughout the CLLC interior.

To verify the successful synthesis of Eu(TTA)$_3$phen inside of porous CLLC scaffold crystals in two solvents, we recorded the photoluminescence emission spectra of individual crystals. Specifically, we used a 20/30 PV™ micro-spectrophotometer (CRAIC) with 365 nm ultraviolet excitation laser beam. The common fixative glutaraldehyde was selected as the cross-linker for the present work due to its high reactivity and general reliability. High glutaraldehyde reactivity and the resulting complex reaction products endow CLLCs with relatively higher auto-fluorescence than other fixatives.[37] To exclude the potential influence of intrinsic fluorescence resulting from crosslinks and solvents for our spectral analysis, we collected fluorescence spectra for control crystals: CLLCs that were respectively soaked in anhydrous ethanol-DMSO mixed solution (Fig. 3a), absolute ethanol (Fig. 3c), and also the emission spectrum of native non-crosslinked HEWL crystal in the original crystallization solution (Fig. 3f). We attribute intrinsic fluorescence to intrinsic protein auto-fluorescence as well as conjugated end products from HEWL glutaraldehyde adducts.[34] While blue emission was quite noticeable in unloaded CLLCs, it was negligible in comparison to the strong red emission peaks for LC-laden CLLCs.

The appearance of intense emission peaks from 4f-4f parity-forbidden transitions provided conclusive evidence that the target lanthanide complex was respectively synthesized or adsorbed within CLLCs. Specifically, the photoluminescence (PL) spectra (Fig. S6) of crystals containing putative LC assembled stepwise in DMSO (sample b in Fig. 3e) or ethanol (sample d Fig. 3e) had the expected strong emission peaks in the 550-750 nm region, in accord with $^5D_0 \rightarrow {}^7F_{J=0,\ 1,\ 2,\ 3,\ 4}$ electronic transitions. LC$^{DMSO\&ethanol}$@CLLC had PL peaks at 579, 590, 612, 651, and 700 nm, while the LC^{ethanol}@CLLC prepared in ethanol

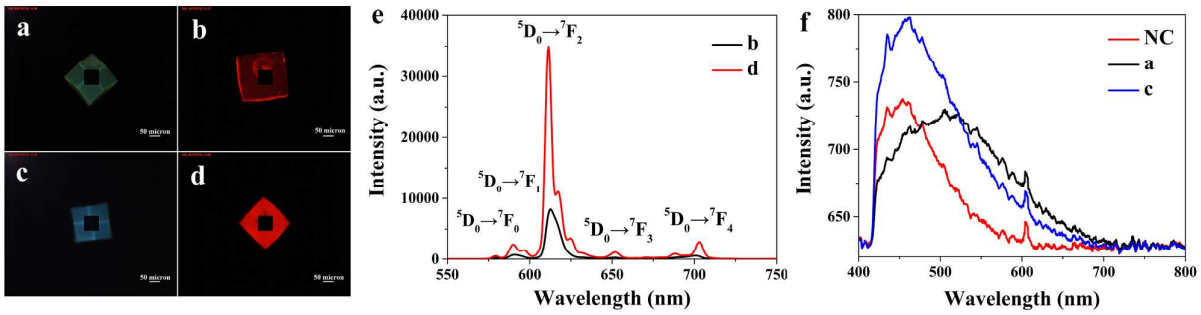

Figure 3. Microspectrophometer results given 365 nm illumination (a) CLLC after denaturation in DMSO and renaturation in ethanol. (b) LC-laden CLLC temporarily expanded in DMSO. (LC$^{DMSO\&ethanol}$@CLLC) (c) CLLC soaked in anhydrous ethanol. (d) LC-laden CLLC where the ligand solvent was anhydrous ethanol. (LC^{ethanol}@CLLC) (e) and (f) show the photoluminescence spectra for the crystals from a-d and one native, non-crosslinked (NC), HEWL crystal. Scale bars in a-d, 50µm.

had PL peaks at 579, 589, 611, 652, and 702 nm. Interestingly, there were several split PL peaks which we rationalize in the following discussion. As is well known, trivalent europium ions have intrinsic extremely low molar absorptivity in the 200-400 nm region due to the forbidden nature of transitions between internal 4f-shells.[38] To ameliorate this deficiency, "antenna" organic ligands[39, 40] such as TTA which possesses distinct molar absorptivity in that region are incorporated into the LC ligand shell. With appropriate antenna ligands, trivalent europium ions are able to efficiently obtain energy from antenna ligands because of the strong coupling between the triplet states to the trivalent ions' emitting levels and subsequently emit intense luminescence. As an aryl-alkyl substituted β-diketone, TTA creates an asymmetric field about the trivalent europium ion, enhancing the efficiency of energy migration to the ion[41] and making radiative transition between the excited state and 7F levels more favorable compared with oscillatory energy dissipation. 1,10-phenanthroline (phen) served as the secondary ligand. One role attributed to phen is the exclusion of water molecules, thereby reducing the probability of thermal dissipation of the triplet state energy via reaction with environmental solvent.[42] The singlet emission peak at 579 nm is associated with a $^5D_0 \rightarrow {}^7F_0$ transition and suggests the formation of only one type of europium complex: $Eu(TTA)_3phen$ in both tested samples. Had more than one peak been evident we might have inferred the presence of isomers or multiple LC species.[43, 44] A $^5D_0 \rightarrow {}^7F_0$ transition can also be indicative of C_{nv}, C_n or C_s symmetry about the Eu^{3+} ion.[45] The $^5D_0 \rightarrow {}^7F_{J=0, 2, 3, 4}$ transitions are easily affected by local electric ligand field. In contrast, the $^5D_0 \rightarrow {}^7F_1$ transition is specifically responsive to the magnetic dipole character, and thus can serve as an internal reference of ligand differences.[46] TTA distorts the idealized O_h symmetry of central europium trivalent ion and induces C_{2v} or lower symmetry of the crystal field about the Eu^{3+} which splits the $^5D_0 \rightarrow {}^7F_1$ transition.[32] Though the number of crystal field components of the $^5D_0 \rightarrow {}^7F_1$ transition of C_{2v} point group symmetry is supposed to be a triplet[47], We observed only an overlapped peak at 590 nm from $LC^{DMSO\&ethanol}$@CLLC and a well separated doublet at 589 nm and 596 nm from$LC^{ethanol}$@CLLC (Fig. 3e).

The most intense emission peak resulted from the $^5D_0 \rightarrow {}^7F_2$ transition, which is also called the electric dipole transition. The $^5D_0 \rightarrow {}^7F_2$ transition is hypersensitive to the surrounding electric field.[43] The intensity of the $^5D_0 \rightarrow {}^7F_4$ transition is also dependent on the environment though it is not as sensitive as the $^5D_0 \rightarrow {}^7F_2$ transtion. Therefore, in the PL spectrum of $LC^{ethanol}$@CLLC, we could find the triplet peaks at 611 nm, 617 nm and 624 nm, which are split from the $^5D_0 \rightarrow {}^7F_2$ transition due to the lower symmetry. In the case of $LC^{DMSO\&ethanol}$@CLLC, only one broad and intense fluorescence band could be seen in its PL spectrum.

The intensity ratio of $^5D_0 \rightarrow {}^7F_2$ to $^5D_0 \rightarrow {}^7F_1$, the monochromaticity value, is commonly used as symmetry indicator for the coordination sphere.[42] The higher the intensity ratio, the more monochromatic the lanthanide complex is and the greater the polarization of the local electric field about the europium trivalent ion.[48] The monochromaticity values for sample b and sample d (Fig. 3e) were 10.66 and 10.69 respectively. Similar monochromaticity for $LC^{DMSO\&ethanol}$@CLLC and $LC^{ethanol}$@CLLC suggests that $Eu(TTA)_3phen$ synthesized in crystals by either route had no obvious difference in their coordination sphere symmetry.

In practice, when observing crystals using fluorescence microscopy it was rather easy to visually discriminate between crystals where LC were aggregated on the surface and crystals where LC were dispersed throughout the interior. However, confocal microscopy is a superior method to show that crystal interiors are loaded, since confocal microscopy allows imaging LC emission from interior crystal planes. Since $Eu(TTA)_3phen$ can be excited at 405 nm (Fig. S7), we were able to use laser scanning confocal microscopy (LSCM) with a 405 nm laser (Olympus, FluoViewTM FV1000). To rule out the role of intrinsic fluorescence from CLLCs (Fig. 3f), we recorded control LSCM images of the same LC-loaded CLLC (Fig4a, 4c) after LC release (Fig. 4b, 4d). Comparing LSCM images in (a), (b) and (c), (d), we noted that LCs ultimately distributed uniformly throughout the crystals (via two approaches).

To quantitatively analyze the process of CLLC denaturation and renaturation in DMSO, we measured CLLC height and width using optical microscopy. To compensate for crystal-to-crystal variability and measurement error, we collected equilibrated crystal dimension data as a function of DMSO concentration for 20 replicated experiments. In principle, CLLCs might experience anisotropic expansion, depending on the extent of molecular expansion across the varying crystallographic interfaces. We observed only minor anisotropy. The most significant difference was a modestly larger maximum expansion of the width (43%) compared to height (28%). The expansion trend for height and the expansion trend for crystal width were fairly similar (Fig. S8a,

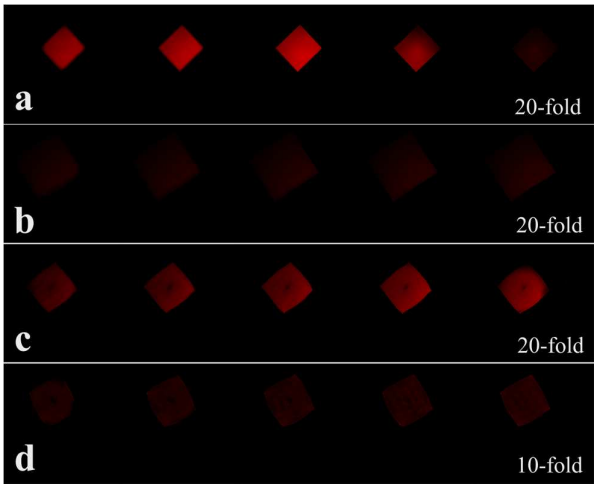

Figure 4. Laser scanning confocal microscopy (LSCM) z-stacks for (a) $LC^{ethanol}$@CLLC, (b) the sample in panel a after LC release, (c) $LC^{DMSO\&ethanol}$@CLLC, and (d) the sample in panel c after LC release. For (a), (b) and (c) the 30 μm z-stack was taken in the middle of the crystal at 7.5 μm intervals. For (d), the 56 μm z-stack was taken in the middle of the DMSO-expanded crystal at 14 μm intervals. 60 minutes in DMSO and anhydrous ethanol mixed solution (V_{DMSO}: $V_{ethanol}$ = 9:1) was used for LC release here. All samples were excited with a 405 nm diode laser.

8b). Therefore, we proceeded to focus on quantifying trends in the expansion of CLLC volume (Fig. 5). We suspect crystal to crystal variability was primarily due to variation in the crosslinking since reactive aldehyde chemistry outcomes can be variable. To assess the uncertainty in the mean relative volume increase, we performed a bootstrap analysis. The error bars in Fig. 5 represent 5% and 95% confidence bounds calculated on the basis of the distribution of mean relative crystal volume values calculated for 10,000 bootstrap datasets resampled with replacement. Hysteresis between expansion and contraction was quite clear.

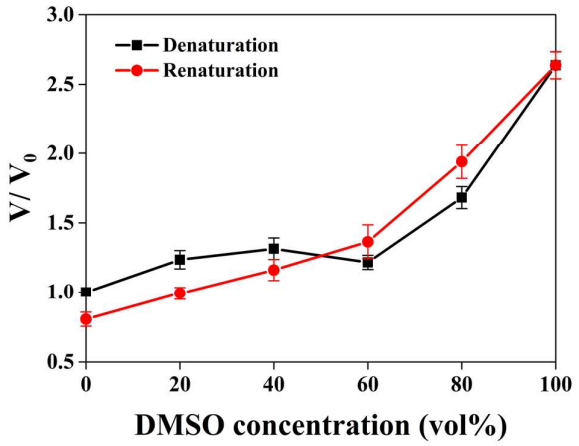

Figure 5. The mean relative volume for the crystals during expansion (black square) and during renaturation (red circle) is displayed, along with the 90% confidence interval for the mean obtained via bootstrap analysis (error bars). The reference V_0 was measured for CLLC soaking in crystallization solution.

Perhaps the most notable feature of Fig. 5 was an apparent crystal size plateau for DMSO concentrations in the 0-60 vol% range. As shown in Fig. 5, CLLCs typically underwent a 25% increase in volume from 0 vol% to 40 vol%, and then stopped expanding (or contracted) after equilibration in 60 vol% DMSO aqueous solution. Non-linear crystal expansion was a consistent feature across all 20 individual crystal trials. Until the concentration of DMSO solution exceeded 60 vol%, we observed only a moderate volume increase for the CLLCs. As the DMSO concentration exceeded 60 vol%, a more dramatic expansion continued until the concentration reached 100%.

Trial-to-trial variation was significant. In 14 out of 23 trials, crystals appeared to undergo a slight contraction in size when equilibrated at 60% DMSO compared to their size when equilibrated at 40% DMSO. Bootstrap analysis suggests that a contraction is not altogether clear from a statistical perspective. Specifically, the upper bound for the confidence interval for relative crystal volume at 60% DMSO is 1.267 and the lower bound for 40% DMSO is 1.237. Therefore, we cannot rule out the possibility that the crystal expansion simply pauses from 40% to 60% rather than reversing.

The biophysical details of solvent-dependent protein denaturation are beyond the scope of the present study, but we note that several papers have analysed the denaturation of HEWL monomers in aqueous DMSO solutions in terms of thermodynamics, energetics, and biophysics.[49-59] HEWL monomers in the solid state, crosslinked to neighbors within a crystal, constitute a significantly different physical system than lysozyme monomers free in solution. Therefore, we cannot assume that the solvent denaturation trends described in early work will translate to the new system. However, we can still note the trends observed in previous work to generate hypotheses.

In particular, these studies mentioned a denaturation threshold for lysozyme monomers at 50-70 vol% (i.e. 20-37 mol%) DMSO that could lend potential insight into the trends observed in Fig. 5. Voets *et al.*[49] used static light scattering and small angle neutron scattering experiments to monitor the static structure factor (S_{90}) and gyration radius (R_g) of lysozyme in aqueous DMSO mixtures as a function of DMSO volume fraction. Their results showed that both S_{90} and R_g were stable prior to a dramatic increase at about 60 vol% DMSO. In contrast, Hamaguchi *et al.*[50] performed UV-vis spectroscopy experiments and reported that the refractive index of the wild-type HEWL interior (surrounding buried tryptophan residues) was found to be close to that of HEWL in 70 vol% DMSO aqueous solution, which implied that lysozyme monomer interior remained similar to the folded state at 70 vol% DMSO concentration.

Intriguingly, non-monotonic DMSO denaturation also has multiple precedents in previous literature. Bagchi *et al.*[51] suggested that up to 15 mol% (40 vol%) DMSO could preferentially solvate the hydrophobic groups of HEWL, causing a partially unfolded HEWL structure without loss of the globular shape. Therefore, only modest volume changes were observed in that range. However, at 15-20 mol% (40-50 vol%) DMSO, the methyl groups of DMSO were hypothesized to switch from solvating the HEWL hydrophobic residues to forming a percolating network near the hydrophobic residues. The local re-organization of solvent molecules accompanied the loss of helical secondary structure of HEWL monomers. It is also possible that HEWL structure collapse occurs at this point, perhaps with the close packing of hydrophobic residues from the helical α-domain. This idea has been figuratively called "hydrophobic zipping"[52]. A similar phenomenon was discovered by P. Balaram *et al.*[53] studying a "protein folding core" structure at 18 mol% DMSO concentration by UV circular dichroism and fluorescence spectroscopic studies. In all, the strong interaction between DMSO and water[54, 55] induced several types of influences on the solvation extent of lysozyme monomers in this binary solvent system at low DMSO concentrations. As the DMSO concentration passed the threshold range of 50-70 vol%, lysozyme monomers unfolded more thoroughly, reaching a higher radius of gyration with increasing DMSO concentration. Tsutomu Arakawa *et al.*[56] described this expansion in thermodynamic terms. Essentially, at higher DMSO concentrations, binding between DMSO and nonpolar residues decreases the free energy of the unfolded protein state, and extensive DMSO binding drives the free energy of the unfolded HEWL state lower than the native state.

Protein refolding is also a complicated process that significantly depends on the local solvent environment. While the volume data includes hysteresis (Fig. 5), we lack the information necessary to postulate a dramatic change in mechanism. HEWL unfolding/denaturation is known to be reversible under some conditions[57]. We tested the extent to which DMSO induced denaturation of the crystalline state was reversible by gradually renaturing our swollen CLLCs. Specifically, we successively transferred CLLCs into aqueous DMSO solutions with 20% lower DMSO concentrations, allowing over 12 hours for equilibration at each DMSO concentration. We concluded the putative renaturation process with incubation in crystallization solution. The final state was noticeably more compact (~20%) than the starting state. This lost volume is consistent with reduced volume for misfolded HEWL monomers, or with a reduced solvent volume. For comparison, classical tetragonal HEWL crystals (e.g. PDB code 193L) have a solvent content of about 40%.[58] One reason the solvent fraction might differ in the final crystals is a change in the composition of the counter ions localized within the crystals, since counter ions were only present during the final equilibration rather than during the entire renaturation process.

Renaturation of HEWL from a DMSO-denatured state has been studied via stopped flow.[59] However, the renaturation of the crystal is likely to differ significantly from renaturation of monomers in solution. Firstly, the timescale for the formation of a collapsed state upon removal of DMSO is milliseconds for proteins in solution, but crystals cannot respond so quickly. Additionally, we suspect that crosslinking to neighboring HEWL monomers in the crystal state will limit the physical extent of unfolding for individual monomers, such that the unfolded state topology is likely to differ from HEWL monomers free in solution. However, it is difficult to make strong inferences about the role of crosslinking when the reactive aldehyde crosslinking process yields stochastic end products.

In the absence of mechanistic details, we envision protein crystal renaturation as a process that is, to a large extent, simply the reverse of denaturation. In other words, an increasing water fraction in the solution will replace DMSO-protein hydrogen bonds with H_2O-protein hydrogen bonds, leading to a solvation shell surrounding the proteins that is enriched in water. To some extent, DMSO will compete with water as a H-bond partner for lysozyme hydrogen bond donor groups. As the DMSO fraction decreases, we expect fewer lysozyme:DMSO H-bonds and a concomitant rise in the number of lysozyme:lysozyme H-bonds and lysozyme:water H-bonds.

During renaturation, as the DMSO concentrations reaches the 50-70 vol% range, we hypothesize that the "hydrophobic zipping" process described by Dill et al. is occurring, rearranging hydrophobic residues and reducing their flexibility concomitant with the formation of hydrophobic cores. The rate of contraction below this concentration range was significantly slower (Fig. 5).

To investigate the effect of LC-loading via different solvent on CLLC microstructure, we used scanning electron microscopy (JSM-7500F, JEOL Ltd.). Micron-scale faults appeared on the surface of the $LC^{DMSO\&ethanol}$@CLLCs surface (Fig. 6c, 6d) as well as the $LC^{ethanol}$@CLLC that was soaked in ligand ethanol solution for several days (Fig. 6e, 6f), but the faults had different forms. For $LC^{DMSO\&ethanol}$@CLLCs, edges in the apex area were relatively flatter and their surfaces were corrugated and reminiscent of orange-peels, with patterns resembling wrinkle-flanked craters perhaps resulting from LC loading (Fig. S9a, 9b). For $LC^{ethanol}$@CLLC, most of the surface was covered with "gooseflesh" patterns (raised islands of approximately 0.5-3 micrometers). Since long-time ethanol incubation made no large differences on the surface of CLLCs (Fig. S9c-f), we attribute the surface patterning to LC loading or possibly the combination of LC loading with the effect of ethanol. The 101, $0\bar{1}1$, $\bar{1}01$ and 011 facets of the control CLLC were flat and smooth at this scale (Fig. 6a, 6b). In contrast, we observed clear hints of irreversible damage in the renatured crystal (Fig. 6g, 6h), despite the gradual, stepwise nature of our renaturation process. This observation is in accord with previous reports of loss of crystallinity during the crosslinking or the denaturation stages.[27] Still, despite tremendous morphological changes at the nanometer and 100-micron scales, CLLCs maintained macro-integrity. To determine

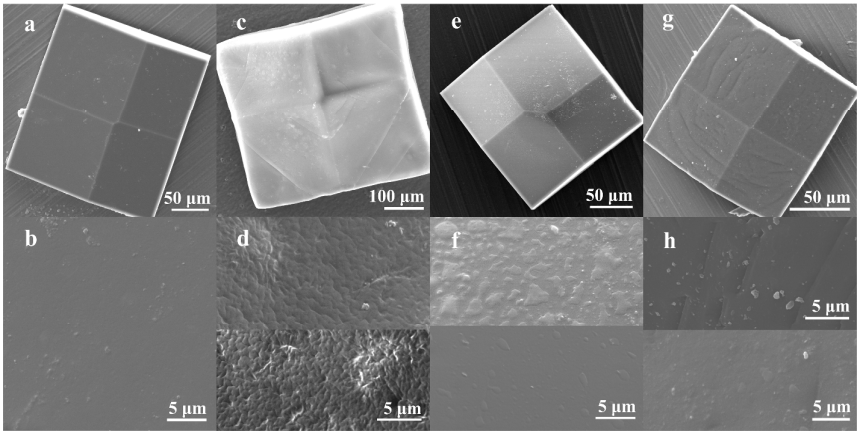

Figure 6. Scanning electron microscopy images: apex area of CLLC (where the 101, $0\bar{1}1$,$\bar{1}01$ and 011 facets meet) for (a) post crosslinking CLLC, (c) $LC^{DMSO\&ethanol}$@CLLC, (e) $LC^{ethanol}$@CLLC, and (g) renatured CLLC; Surface details of apex area of (b) CLLC from panel a, (d) two surface close-ups from panel c, (f) two surface close-ups from panel e, (h) two surface close-ups from from panel g. All samples were dried in vacuum at 20℃ overnight and treated by gold sputtering.

whether it was feasible to study these materials via single-crystal X-ray diffraction (XRD), we incubated a glutaraldehyde crosslinked crystal in 100% ethanol for 48 hours and collected XRD using a Rigaku HomeLab with a microfocus X-ray generator and a Pilatus 200K detector (Fig. S10).

Due to a lack of intrinsic contrast, the necessity of vacuum conditions, and the disadvantageous properties of soft materials for standard microtome sample preparation, it is quite challenging to observe the native porous nanostructure of protein crystals via transmission electron microscopy. Normal methods for the preparation of biological material samples may involve contrast reagents like OsO_4 or the use of solvents like water or acetone, solvents in which LC could readily diffuse out of a protein crystal layer obtained via microtome. Additionally, an expansion and contraction cycle will further decrease the likelihood of observing an intact periodic array via TEM or HRTEM. In our attempts, embedding $LC^{ethanol}$@CLLCs in epoxy resin, no obviously periodic array of heavy lanthanide clusters was observed within 100 nm ultrathin CLLC layers (Fig. S11a-c). However, the corresponding EDX spectrum had peaks assigned to Europium (Fig. S11d).

Considering the EDX data (Fig. S11d), together with the confocal images (Fig. 4), and the pertinent microspectrophotometer luminescence spectra (Fig. 3e, S7), we conclude that Eu(TTA)3phen was successfully synthesized in crystallo. The present work conclusively demonstrates that CLLCs can serve as a host matrix material for the synthesis and gradual release of guest LCs.

Conclusions

The work herein describes several hitherto unobserved phenomena. First, cross-linked HEWL crystals were expanded, on average, to a 2.5-fold greater volume in DMSO and could be restored to minimal volumes via gradual renaturation. Second, $Eu(TTA)_3$phen complexes could be constituted inside of host protein crystals by first loading the crystals with the hydrophobic ligands phen and TTA in DMSO or anhydrous ethanol and subsequently loading Eu(III) in anhydrous ethanol. Third, we used SEM to observe micro-scale changes (surface faults and alterations) in cross-linked HEWL crystals that underwent guest loading or expansion. Fourth, we have observed qualitative differences in the rate of LC escape from host crystals in three solvents.

Considering these results as a whole, we can assess the potential of protein crystals as host materials for hybrid materials, and flag the most critical questions for follow-on research. The expansion of CLLCs in DMSO here provides an interesting option for the preparation of future hybrid materials in which the guest molecules are highly hydrophobic or where the guest molecules are too large for diffusion into native crosslinked HEWL crystals. For the specific task of organizing an array of guest molecules that interact with light, it would be advantageous to use an alternative protein crystal scaffold with somewhat larger pores to facilitate the diffusion of the constituent dyes or fluorophores. If on the other hand, the goal is to entrap non-covalently bound small molecules, the HEWL crystals used here may be favourable. Ultimately, the relatively small solvent pores in tetragonal HEWL crystals (Fig. 1) likely slowed the release of LC payloads in water and ethanol solvents.

In the long term, it would be desirable to test alternative protein crystal scaffolds to the commonly-used HEWL that have differing solvent channel topology, and could therefore provide a different spatial organization of functional guest molecules. For example, it could be desirable to use a scaffold protein crystal composed of a thermophilic protein building block, or a crystalline packing arrangement that leads to a high solvent fraction for greater capacity. Second, it would be desirable to identify alternative or supplemental crosslinking agents to the commonly-used glutaraldehyde that might provide the resulting cross-linked protein crystals with greater macroscopic stability with respect to organic solvents. Materials capable of such dramatic changes in volume that are simultaneously robust with respect to a large number of expansion and contraction cycles might find interesting new uses. It may also be possible to alter the crosslinking chemistry to provide the resulting crystals with superior physico-chemical properties for the immobilization of the guest molecules of interest.

Conflicts of interest

There are no conflicts of interest to declare.

Acknowledgements

This work was supported by (1) The Natural Scientific Foundation of China (Grant No. 51473082), (2) The National Scientific Foundation of the USA, Nanomaterials Grant No. 1434786 (3) The Program for Introducing Talents of Discipline to Universities (“111” plan); (4) State Key Project of International Cooperation Research (2016YFE0110800, 2017YFE0108300); (5) The 1st class disciplines of Shandong Province; (6) The National One-Thousand Foreign Expert Program (Grant No. WQ20123700111).

References

1. C. R. Simmons, F. Zhang, T. MacCulloch, N. E. Fahmi, N. Stephanopoulos, Y. Liu and H. Yan, Acta Crystallographica Section A: Foundations and Advances, 2017, 73, a53-a53.
2. E. M. Puchner, S. K. Kufer, M. Strackharn, S. W. Stahl and H. E. Gaub, Nano Letters, 2008, 8, 3692-3695.
3. A. E. Kowalski, T. R. Huber, T. W. Ni, L. F. Hartje, K. L. Appel, J. W. Yost, C. J. Ackerson and C. D. Snow, Nanoscale, 2016, 8, 12693-12696.
4. T. R. Huber, E. C. Mcpherson, C. E. Keating and C. D. Snow, Bioconjugate Chemistry, 2017, 29, 17-22.
5. L. F. Hartje, B. E. Munsky, T. W. Ni, C. J. Ackerson and C. D. Snow, Journal of Physical Chemistry B, 2017, 121, 7652-7659.

6. T. Koshiyama, N. Kawaba, T. Hikage, M. Shirai, Y. Miura, C. Y. Huang, K. Tanaka, Y. Watanabe and T. Ueno, Bioconjugate Chemistry, 2010, 21, 264-269.
7. C. J. Lusty, Journal of applied crystallography, 1999, 32, 106-112.
8. J. A. Kiernan, Microscopy today, 2000, 1, 8-12.
9. X. P. Yang, B. S. Kang, W. K. Wong, C. Y. Su and H. Q. Liu, Inorganic Chemistry, 2003, 42, 169-179.
10. M. H. V. Werts, R. T. F. Jukes and J. W. Verhoeven, Physical Chemistry Chemical Physics, 2002, 4, 1542-1548.
11. N. Sabbatini, M. Guardigli and J. M. Lehn, Coordination Chemistry Reviews, 1993, 123, 201–228.
12. G. F. D. Sá, O. L. Malta, C. D. M. Donegá, A. M. Simas, R. L. Longo, P. A. Santa-Cruz and E. F. D. S. Jr, Coordination Chemistry Reviews, 2000, 196, 165-195.
13. S. W. Magennis, S. Parsons, Z. Pikramenou, A. Corval and J. D. Woollins, Chemical Communications, 1999, 1, 61-62.
14. S. Faulkner, S. J. A. Pope and B. P. Burton‐Pye, Applied Spectroscopy Reviews, 2005, 40, 1-31.
15. A. P. De Silva, H. Q. N. Gunaratne and T. E. Rice, Angewandte Chemie International Edition in English, 1996, 35, 2116-2118.
16. L. Armelao, S. Quici, F. Barigelletti, G. Accorsi, G. Bottaro, M. Cavazzini and E. Tondello, Coordination Chemistry Reviews, 2010, 254, 487-505.
17. P. Lenaerts, A. Storms, J. Mullens, J. D'Haen, C. Görller-Walrand, K. Binnemans and K. Driesen, Chemistry of materials, 2005, 17, 5194-5201.
18. L. I. Zongren, X. I. Peng, M. Zhao, G. U. Xiaohua, M. A. Qiaoyu and B. Cheng, Journal of Rare Earths, 2010, 28, 211-214.
19. A. Freeman, Biomimetics, 2017, 2, 14.
20. N. Cohen-Hadar, Y. Wine, E. Nachliel, D. Huppert, M. Gutman and A. Freeman, Biotechnology & Bioengineering, 2006, 94, 1005-1011.
21. T. Ueno, Chemistry (Weinheim an der Bergstrasse, Germany), 2013, 19, 9096-9102.
22. N. Dotan, D. Arad and A. Freeman, Angewandte Chemie International Edition, 1999, 38, 2363-2366.
23. M. Guli, M. Li, Z. Hu, J. Yao and S. Mann, Journal of Materials Science, 2015, 50, 7026-7030.
24. M. W. England, A. J. Patil and S. Mann, Chemistry, 2015, 21, 9008-9013.
25. M. Guli, E. M. Lambert, M. Li and S. Mann, Angew Chem Int Ed Engl, 2010, 49, 520-523.
26. A. Cvetkovic, A. J. J. Straathof, R. Krishna and L. A. M. V. D. Wielen, Langmuir the Acs Journal of Surfaces & Colloids, 2005, 21, 1475-1480.
27. D. J. Haas, Biophysical Journal, 1968, 8, 549-555.
28. A. Yonath, A. Podjarny, B. Honig, A. Sielecki and W. Traub, Biochemistry, 1977, 16, 1418-1424.
29. A. Yonath, A. Podjarny, B. Honig, W. Traub, A. Sielecki, O. Herzberg and J. Moult, Biophysics of Structure & Mechanism, 1977, 4, 27-36.
30. M. C. Vaney, S. Maignan, M. Riès-Kautt and A. Ducruix, Acta Crystallographica, 1996, 52, 505-517.
31. D. H. Juers and J. Ruffin, Journal of Applied Crystallography, 2014, 47, 2105-2108.
32. H. Mao‐Lin, H. Zhen‐Yan, C. Ya‐Qian, W. Shm, L. Juan‐Juan, H. Yi, X. Duan‐Jun and X. Yuan‐Zhi, Chinese Journal of Chemistry, 1999, 17, 637-643.
33. I. Migneault, C. Dartiguenave, M. J. Bertrand and K. C. Waldron, Biotechniques, 2004, 37, 798-802.
34. K. Lee, S. Choi, C. Yang, H. C. Wu and J. Yu, Chemical Communications, 2013, 49, 3028-3030.
35. A. Cvetkovic, C. Picioreanu, A. J. Straathof, R. Krishna and V. D. W. La, Journal of the American Chemical Society, 2005, 127, 875-879.
36. L. F. Hartje, B. E. Munsky, T. W. Ni, C. J. Ackerson and C. D. Snow, Journal of Physical Chemistry B, 2017, 121 7652-7659.
37. J. B. Pawley and B. R. Masters, Journal of Biomedical Optics, 2008, 13, 2766.
38. B. JC and P. C, Chemical Society Reviews, 2005, 34, 1048-1077.
39. J. Pei, X.-L. Liu, W.-L. Yu, Y.-H. Lai, Y.-H. Niu and Y. Cao, Macromolecules, 2002, 35, 7274-7280.
40. F. Liang, Q. Zhou, Y. Cheng, L. Wang, D. Ma, A. Xiabin Jing and F. Wang, Chemistry of Materials, 2003, 15, 1935-1937.
41. N. Filipescu, W. Sager and F. Serafin, The Journal of Physical Chemistry, 1964, 68, 3324-3346.
42. P. K. Shahi, A. K. Singh, S. K. Singh, S. B. Rai and B. Ullrich, Acs Appl Mater Interfaces, 2015, 7, 18231-18239.
43. F. S. Richardson, Chemical Reviews, 1982, 82, 541-552.
44. L. Melby, N. Rose, E. Abramson and J. Caris, Journal of the American Chemical Society, 1964, 86, 5117-5125.
45. K. Binnemans and C. Görller-Walrand, Journal of rare earths, 1996, 14, 173-180.
46. J.-C. Bünzli and G. R. Choppin, 1989.
47. K. Binnemans, Coordination Chemistry Reviews, 2015, 295, 1-45.
48. A. K. Singh, S. K. Singh, H. Mishra, R. Prakash and S. B. Rai, Journal of Physical Chemistry B, 2010, 114, 13042-13051.
49. I. K. Voets, W. A. Cruz, C. Moitzi, P. Lindner, E. P. G. Arêas and P. Schurtenberger, Journal of Physical Chemistry B, 2010, 114, 11875-11883.
50. K. Hamaguchi and K. Imahori, Journal of Biochemistry, 1964, 55, 388-393.
51. S. Roy, B. Jana and B. Bagchi, Journal of Chemical Physics, 2012, 136, 03B608.
52. K. A. Dill, K. M. Fiebig and H. S. Chan, Proceedings of the National Academy of Sciences of the United States of America, 1993, 90, 1942-1946.
53. S. Bhattacharjya and P. Balaram, Proteins-structure Function & Bioinformatics, 2015, 29, 492-507.
54. C. F. Lau, P. T. Wilson and D. V. Fenby, Australian Journal of Chemistry, 1970, 23, 1143-1148.
55. R. N. Havemeyer, Journal of Pharmaceutical Sciences, 1966, 55, 851-853.
56. T. Arakawa, Y. Kita and S. N. Timasheff, Biophysical Chemistry, 2007, 131, 62-70.
57. M. Kotik, S. E. Radford and C. M. Dobson, Biochemistry, 1995, 34, 1714-1724.
58. J. D. Schmit and K. A. Dill, Journal of Physical Chemistry B, 2010, 114, 4020-4027.
59. S. C. Mande and M. E. Sobhia, Protein Engineering, 2000, 13, 133-141.

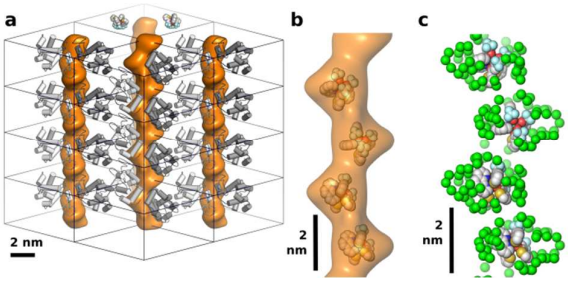

$Eu(TTA)_3phen$ was synthesized inside of crosslinked protein crystals. And we characterized the volumetric changes quantitatively induced by DMSO.